ARTICLE

Insights into the catalytic mechanism of a bacterial deglycase essential for utilization of fructose-lysine

Sravya Kovvali[1,2] | **Yuan Gao**[2,3] | **Austin Cool**[2] | **Steffen Lindert**[2] ⓘ |
Vicki H. Wysocki[2,3] ⓘ | **Charles E. Bell**[2,4] ⓘ | **Venkat Gopalan**[1,2] ⓘ

[1]Department of Microbiology, The Ohio State University, Columbus, Ohio, USA

[2]Department of Chemistry & Biochemistry, The Ohio State University, Columbus, Ohio, USA

[3]Resource for Native MS-Guided Structural Biology, The Ohio State University, Columbus, Ohio, USA

[4]Department of Biological Chemistry & Pharmacology, The Ohio State University, Columbus, Ohio, USA

Correspondence
Vicki H. Wysocki, Department of Chemistry & Biochemistry, The Ohio State University, Columbus, OH 43210, USA.
Email: wysocki.11@osu.edu

Charles E. Bell, Department of Biological Chemistry & Pharmacology, The Ohio State University, Columbus, OH 43210, USA.
Email: bell.489@osu.edu

Venkat Gopalan, Department of Chemistry & Biochemistry, The Ohio State University, Columbus, OH 43210, USA.
Email: gopalan.5@osu.edu

Funding information
National Institutes of Health, Grant/Award Numbers: P41-GM128577, NIAID R01-AI140541

Review Editor: Aitziber L. Cortajarena

Abstract

Amadori rearrangement products are stable sugar-amino acid conjugates that are formed nonenzymatically during preparation, dehydration, and storage of foods. Because Amadori compounds such as fructose-lysine (F-Lys), an abundant constituent in processed foods, shape the animal gut microbiome, it is important to understand bacterial utilization of these fructosamines. In bacteria, F-Lys is first phosphorylated, either during or after uptake to the cytoplasm, to form 6-phosphofructose-lysine (6-P-F-Lys). FrlB, a deglycase, then converts 6-P-F-Lys to L-lysine and glucose-6-phosphate. Here, to elucidate the catalytic mechanism of this deglycase, we first obtained a 1.8-Å crystal structure of *Salmonella* FrlB (without substrate) and then used computational approaches to dock 6-P-F-Lys on this structure. We also took advantage of the structural similarity between FrlB and the sugar isomerase domain of *Escherichia coli* glucosamine-6-phosphate synthase (GlmS), a related enzyme for which a structure with substrate has been determined. An overlay of FrlB—6-P-F-Lys on GlmS—fructose-6-phosphate structures revealed parallels in their active-site arrangement and guided our selection of seven putative active-site residues in FrlB for site-directed mutagenesis. Activity assays with eight recombinant single-substitution mutants identified residues postulated to serve as the general acid and general base in the FrlB active site and indicated unexpectedly significant contributions from their proximal residues. By exploiting native mass spectrometry (MS) coupled to surface-induced dissociation, we distinguished mutations that impaired substrate binding versus cleavage. As demonstrated with FrlB, an integrated approach involving x-ray crystallography, in silico approaches, biochemical assays, and native MS can synergistically aid structure–function and mechanistic studies of enzymes.

KEYWORDS
Amadori compound, catalytic mechanism, FrlB deglycase, fructose-lysine metabolism

1 | INTRODUCTION

The nonenzymatic Maillard reaction occurs during frying, drying, and roasting and contributes to the color, flavor, and taste of foods (Nursten, 1981). Amadori rearrangement products are the first stable compounds formed during this reaction (Mossine & Mawhinney, 2010). The condensation between an amino group present in an amino acid and a carbonyl group of a reducing sugar results in an unstable Schiff base, which then rearranges to form the more stable Amadori compound (e.g., glucose + lysine yields fructose-lysine [F-Lys]).

Amadori compounds occur widely in nature and are of clinical and nutritional significance. For example, the reaction of glucose with free amines in plasma proteins is used to diagnose hyperglycemia (Lenters-Westra et al., 2013; McFarland et al., 1979). Transformation of the Amadori compounds to dicarbonyl derivatives leads to advanced glycation end products, which have been linked to inflammation and disease (Nursten, 1981). The human diet routinely includes Amadori compounds: for example, F-Lys in dried carrots, chocolates, and oat flakes (Erbersdobler & Faist, 2001; Erbersdobler & Somoza, 2007; Mossine & Mawhinney, 2010); F-Glu in tomato paste or powder (Mossine & Mawhinney, 2010); F-Asn in dried apricots and apples (Wu et al., 2018). Interestingly, recent studies (van Dongen et al., 2022; Wolf et al., 2019) highlight how dietary F-Lys could reshape the gut microbiota. Because F-Lys is nearly absent in breast milk, yet present in high amounts in formula milk (Erbersdobler & Faist, 2001; Martysiak-Żurowska & Stołyhwo, 2007), one investigation (van Dongen et al., 2022) compared breast-fed and formula-fed infants for their respective gut microbial F-Lys degradation activity. Indeed, the feces of formula-fed infants had more F-Lys-metabolizing bacteria of different taxa (van Dongen et al., 2022). Another study found that *Intestinimonas butyriciproducens*, the only gut bacterium known to convert F-Lys to butyrate (Bui et al., 2015), was more prevalent in the feces of formula-fed infants (Bui et al., 2020). In addition to uncovering human gut microbiota variations that dictate F-Lys assimilation differences, it is important to understand the microbial enzymes and pathways that permit F-Lys utilization.

There are three different routes used by prokaryotes and eukaryotes for catabolism of Amadori compounds (Van Schaftingen et al., 2012). The first strategy, which is prevalent in fungi, consists of oxidases (amadoriases) that convert fructosamines to glucosone, peroxide, and the respective amino acids. The second option, which is found in several eukaryotes, employs fructosamine-3-kinases to convert fructosamines to fructosamine-3-phosphates that spontaneously disintegrate owing to their inherent instability. The third path, which is predominantly used by bacteria, comprises a kinase that phosphorylates the fructosamine to form the corresponding 6-phospho-fructosamine that is then cleaved by a deglycase into glucose-6-phosphate (Glc-6-P) and the corresponding amino acid. There are some variations to the first step in this pathway (Deppe, Bongaerts, et al., 2011; Wiame et al., 2002, 2004). For instance, a phosphotransferase system couples the transport and phosphorylation of F-Lys in *Salmonella enterica* serovar Typhimurium (referred hereafter as *Salmonella*; Miller et al., 2015), whereas a dedicated transporter and a kinase are used in *Escherichia coli* (Deppe, Klatte, et al., 2011; Wiame & Van Schaftingen, 2004; Figure S1). The FrlB deglycase, however, is the common endpoint that converts 6-phosphofructose-lysine (6-P-F-Lys) to L-lysine and Glc-6-P, thus yielding ATP and metabolic intermediates.

Although FrlB is the focus of this study, FraB, a related deglycase, has recently been identified as a novel drug target since disrupting the FraB-dependent metabolism of F-Asn by *Salmonella* results in the accumulation of a toxic sugar-phosphate metabolite (Sabag-Daigle et al., 2016). To this end, we have invested much effort to design a narrow-spectrum therapeutic to inhibit *Salmonella* FraB (Sabag-Daigle et al., 2023; Thirugnanasambantham et al., 2022). Our interest in FraB inspired our studies of the catalytic mechanism of *Salmonella* FrlB. Comparisons of the FrlB and FraB active sites would be a first step to understand the deglycase specificity determinants for ε- (6-P-F-Lys) versus α- (6-phosphofructose-aspartate, 6-P-F-Asp) glycated substrates.

Here, we determined the crystal structure of FrlB, which revealed its tertiary fold, dimeric arrangement, and putative active site. However, our inability to obtain a structure of FrlB bound to its substrate 6-P-F-Lys precluded immediate insights into catalysis. Therefore, we utilized computational docking to position 6-P-F-Lys on FrlB and probed the resulting model using structural alignments of FrlB with glucosamine-6-phosphate synthase (GlmS), a distant homolog (Wiame et al., 2002) for which the structure of a substrate complex is available (Durand et al., 2008). The strong correspondence between the FrlB and GlmS active sites, evident from a comparison of the two substrate-bound structures, helped us to select residues for mutagenesis. To determine if FrlB mutants are inactive due to defects in either substrate binding or cleavage, we coupled biochemical assays with native mass spectrometry (MS) studies; results from this combined approach uncovered differences in roles played by certain amino acid residues that we postulated to contribute equally to substrate binding. Using FrlB as an example, we demonstrate the value of integrating crystallography, in silico

approaches, enzyme assays, and native MS to elucidate enzyme mechanisms.

2 | RESULTS

2.1 | High-resolution crystal structure of *Salmonella* FrlB

To understand the catalytic mechanism of *Salmonella* FrlB, we first sought to obtain its high-resolution structure. *Salmonella* FrlB was overexpressed in *E. coli* and purified to near homogeneity using affinity chromatography (Figure S2). We then obtained a 1.8-Å crystal structure of FrlB in the absence of substrate (Table 1). We solved the FrlB structure by molecular replacement using a putative glucosamine-fructose-6-phosphate aminotransferase (GFAT; PDB: 2A3N, unpublished) as the search model. Although the asymmetric unit of the crystal contains only one chain of FrlB, a FrlB dimer that is similar to the GFAT dimer can be generated in COOT by applying a 2-fold crystal symmetry (Figures 1 and S3). Multiple rounds of refinement and model building yielded final R factors and free R factors of 0.160 and 0.203, respectively (Table 1). The electron density around the putative catalytic center was well defined, and the final model consists of 2508 protein atoms, 238 water molecules, and 6 atoms from a glycerol molecule bound to the protein. Our attempts to co-crystallize FrlB with 6-P-F-Lys (substrate) and Glc-6-P (product) were not successful.

The FrlB monomer folds into two subdomains, each with a similar three-layer (αβα) sandwich-type fold, with several alternating α helices and β strands. (Figures 1 and S3). *Salmonella* FraB, a deglycase like FrlB, and other sugar isomerases utilize a general acid (His) and general base (Glu) to catalyze their respective reactions via enediol intermediates (Figure S4; Sengupta et al., 2019; Teplyakov et al., 1999). FraB forms a homodimer even at 20 nM and likely functions as a dimer in vivo (Sengupta et al., 2019). Therefore, we propose that FrlB also functions as a dimer (see supporting MS data below). Additionally, each dimer has two active sites, with the two putative catalytic residues (E224 and H240) coming together from separate monomers to form each active site at the dimer interface (Figure 1a). It is unknown if the two active sites operate independently from one another or in a concerted manner.

The surface electrostatic potential map of FrlB (Figure 1b) generated using Chimera (Pettersen et al., 2021) reveals a positively charged cleft formed by R267, R270, and K274. This cleft is adjacent to the active-site pocket and could guide the negatively charged 6-P-F-Lys substrate to the active site. We also used CASTp

(Computed Atlas of Surface Topography of proteins; Tian et al., 2018) to delineate a concave cavity that overlaps with the active site (Figure 1c). The active site is solvent exposed, with a volume of about 600 Å^3 and a surface area of ~430 Å^2.

2.2 | Multiple sequence alignment for FrlB

Conserved amino acid residues in orthologs or homologs are often indicative of their functional significance. To identify additional conserved residues in FrlB, we used DeepMSA2, an open-source multiple sequence alignment

TABLE 1 Data collection and refinement statistics.

Data collection	
Space group	P2(1)2(1)2
Cell dimensions	
a, b, c, Å	53.68, 75.22, 82.84
α, β, γ, °	90, 90, 90
Resolution, Å	45.1–1.83 (1.88–1.83)
Rmerge	0.091 (0.511)
I/σI	20.5 (3.7)
Completeness, %	94.3 (84.7)
Redundancy	5.5 (5.2)
Refinement	
Resolution, Å	45.1–1.80
Number of reflections	28,564
Rwork/Rfree	0.160/0.203
Number of atoms	
Protein	2506
Water	238
Ligand	6
B factors, Å^2	
Protein	17.1
Water	28.0
Ligand	25.0
RMSD	
Bond lengths, Å	0.011
Bond angles, °	1.66
Ramachandran plot	
Favored, *n* (%)	307 (98)
Allowed, *n* (%)	10 (2)
Outliers	0

Note: Diffraction data were collected from a single crystal. Coordinates have been deposited to the Protein Data Bank (accession code 8GLR).
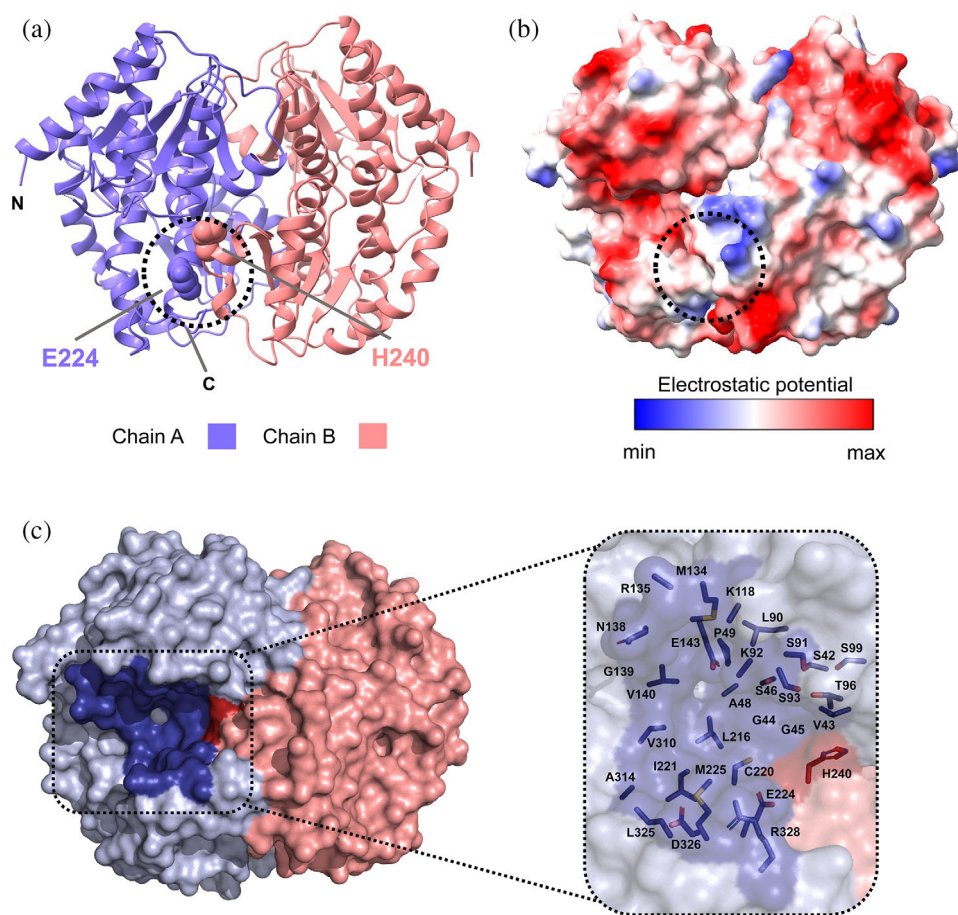Abbreviation: RMSD, root mean square deviation.

FIGURE 1   Crystal structure of *Salmonella* FrlB. (a) The two chains of the FrlB dimer are colored differently (A, blue; B, pink) with the N- and C-termini indicated for Chain A. The intersubunit active site comprised of E224 from Chain A and H240 from Chain B is depicted. (b) Electrostatic potential map of the FrlB dimer generated using UCSF ChimeraX (Pettersen et al., 2021). In both panels, the active site is encircled in black dashed lines. A second active site formed by H240 of Chain A and E224 of Chain B is located on the posterior of the dimer. Coordinates for *Salmonella* FrlB have been deposited to the Protein Data Bank (accession code 8GLR). (c) Surface view of FrlB depicting the CASTp (Tian et al., 2018)-predicted solvent-exposed cavity (dark blue) that overlaps the active site; inset shows the residues that line the cavity.

(MSA) pipeline that is an extension of DeepMSA (Zhang et al., 2020). Traditional MSA tools build alignments relying on user-provided sequences of homologs; such an approach could (i) introduce bias due to inclusion of highly similar sequences, and (ii) lower the accuracy of the alignment if partial or incomplete sequences were inadvertently included. These shortcomings are addressed by DeepMSA2, an automated pipeline that provides more robust MSAs by selecting sequences with higher diversity. Moreover, rather than depend only on National Center for Biotechnology Information (NBCI), DeepMSA2 uses whole genome and metagenome databases and thereby provides superior coverage and depth through a hybrid homology-detection approach.

When we used *Salmonella* FrlB as the query sequence on the DeepMSA2 online server, it generated a sequence logo from an MSA comprising ~6400 homologs (Figure S5A). The residues E224 and H240 are highly conserved in most deglycases, including the FraB deglycase involved in F-Asn metabolism (Sengupta et al., 2019). Remarkably, these two nearly universally conserved residues are always spaced 16 residues apart in the linear sequence despite the fact that each active site in the homodimer is generated with the Glu from one monomer and the His from the other. Based on our previous mutagenesis studies of FraB (when we observed that E214A, E214D, and H230A were completely inactive; Sengupta et al., 2019), we posited that the equivalent residues in FrlB (E224 and H240) are likely to be essential for cleavage of 6-P-F-Lys (Figure S4). While these two residues were primary candidates for mutagenesis, we sought to better define the catalytic center in FrlB through a computational approach given the absence of an enzyme–substrate (ES) crystal structure. Apart from E224 and H240, the MSA analysis helped identify other highly conserved residues that could serve as potential candidates for mutagenesis studies—S46, S91, S93, G94, T96, E98, E224, and H240 (Figure S5A). Because many of these conserved residues were observed to be clustered in the active-site pocket (see below), we postulated a role for them in substrate binding but sought additional support before initiating mutagenesis studies.

2.3 | Molecular dynamics simulations

We performed computational docking and molecular dynamics (MD) simulations on FrlB. The FrlB crystal structure was subjected to a 50-ns MD simulation to investigate the dynamics of the free enzyme. After 6-P-

F-Lys was docked into the FrlB crystal structure using Glide Standard Precision (SP; Figure S6A), this model of the ES complex was subjected to a 50-ns MD simulation. We observed that in a few frames, including the 20 ns-frame of the simulation, the 6-P-F-Lys molecule folded upon itself, allowing the Lys moiety in the substrate to interact with specific residues in FrlB (e.g., S93 in the loop that connects β3 and α5; Figure S6C). The position of the Lys moiety drastically changed from its initial binding pose during the simulation, as evident from an all-atom root mean square deviation (RMSD) calculation of the 6-P-F-Lys to its starting position (Figure S6F). In contrast to the amino acid, the sugar moiety remained stable throughout the simulation, thus lending confidence to its pose. Notably, visual inspection of both the MD trajectories (i.e., in the absence or presence of substrate; Figure S6B,D) revealed that there were no major shifts in the tertiary structure of the FrlB dimer or even the active site during the entire duration of the simulation. The global RMSD of the backbone atoms never exceeded a value of 1.6 Å when compared with the starting model, and the active-site RMSD did not exceed 2.0 Å. Evaluation of the root mean square fluctuation (RMSF) of all residues did not indicate large fluctuations of any residues involved in the active site throughout the 50-ns trajectory of free FrlB (Figure S6E).

The 50-ns MD simulation of FrlB—6-P-F-Lys produced 25,000 frames to analyze. For each of these frames, the FrlB residues that were in contact with 6-P-F-Lys were determined. The results for the fraction of 25,000 frames with residue-ligand contacts for >25 ns are shown in Table S1. Only one of the two inter-subunit active sites was used for the MD simulations, and Chain A refers to the monomer with E224 whereas Chain B refers to the monomer with H240. All the residues in Table S1 are from Chain A except H240 which was located on Chain B. These 6-P-F-Lys–interacting residues are clustered into three distinct segments of FrlB: residues 43–46, 90–99, and 216–224. Several residues from these segments in FrlB (S46, S91, S93, T96, E224, and H240) coincide with highly conserved residues identified in the MSA (Figure S5A), thus justifying their choice for mutagenesis. The remaining residues from Table S1 were not conserved among the deglycases and GlmS homologs and/or distal from the active-site pocket in our crystal structure.

2.4 | Structural alignment of FrlB with a glucosamine-6-phosphate synthase

Towards our goal of identifying the active-site residues in FrlB that are important for to 6-P-F-Lys recognition, we sought additional insights from structural comparisons.

Previous studies have suggested that deglycases, including Salmonella FrlB, may be distantly related to GlmS, which is an essential and ubiquitous enzyme central to hexosamine metabolism (Wiame et al., 2005). These enzymes exist as dimers in prokaryotes and as tetramers in eukaryotes (Milewski, 2002). GlmS is composed of an isomerase domain and a glutaminase domain; the latter hydrolyzes glutamine to form glutamate and ammonia. The ammonia is transferred via a channel to the isomerase domain for incorporation with fructose-6-phosphate (Fru-6-P) to form glucosamine-6-phosphate (Teplyakov et al., 2001). In the absence of glutamine, E. coli GlmS catalyzes the isomerization of Fru-6-P into Glc-6-P (Teplyakov et al., 1999). GlmS homologs as well as the FrlB/FraB deglycases are similar in that they both possess a sugar isomerase (SIS) domain and contain the key Glu and His catalytic residues, positioned exactly 16 amino acids apart (Figure S5A,B).

To assess if GlmS could provide clues to better understand FrlB catalysis, we used the align function of PyMOL to perform a structural overlay of E. coli GlmS + Fru-6-P (PDB: 4AMV; Durand et al., 2008) and our Salmonella FrlB structure on which 6-P-F-Lys had been docked (Figure S6A). This superposition (RMSD, 2.87 Å; Figure 2) revealed strong agreement between the SIS domains of these two enzymes, an unexpected finding given that E. coli GlmS and Salmonella FrlB share only ~20% sequence identity and ~45% sequence similarity across the SIS domains. The putative general base (E224) and general acid (H240) in FrlB are closely aligned with the E488 and H504 counterparts in GlmS; likewise, S46, S91, S93, and T96 from FrlB align with their counterparts in GlmS (Figure 2). There are some differences that are meaningful in the context of each structure. For example, E98 in FrlB is ~3 Å from the putative general acid, H240, an observation that motivates our hypothesis that E98 positions H240 for optimal catalytic activity. However, in the case of GlmS, the corresponding residue for E98 is D354, which is not positioned proximally to the catalytic H504. Despite this difference, we decided to mutate FrlB E98 because of its proximity H240, the putative general acid. Overall, this exercise comparing FrlB and GlmS led us to choose S46, S91, S93, T96, E98, E224, and H240 in FrlB for mutagenesis and follow-up studies.

2.5 | Mutagenesis and characterization of the FrlB mutants

Using site-directed mutagenesis, we generated eight mutants: S46A, S91A, S93A, T96A, E98A, E224A, E224Q, and H240A. In addition to seven alanine substitution mutants, we constructed E224Q since Gln is a polar
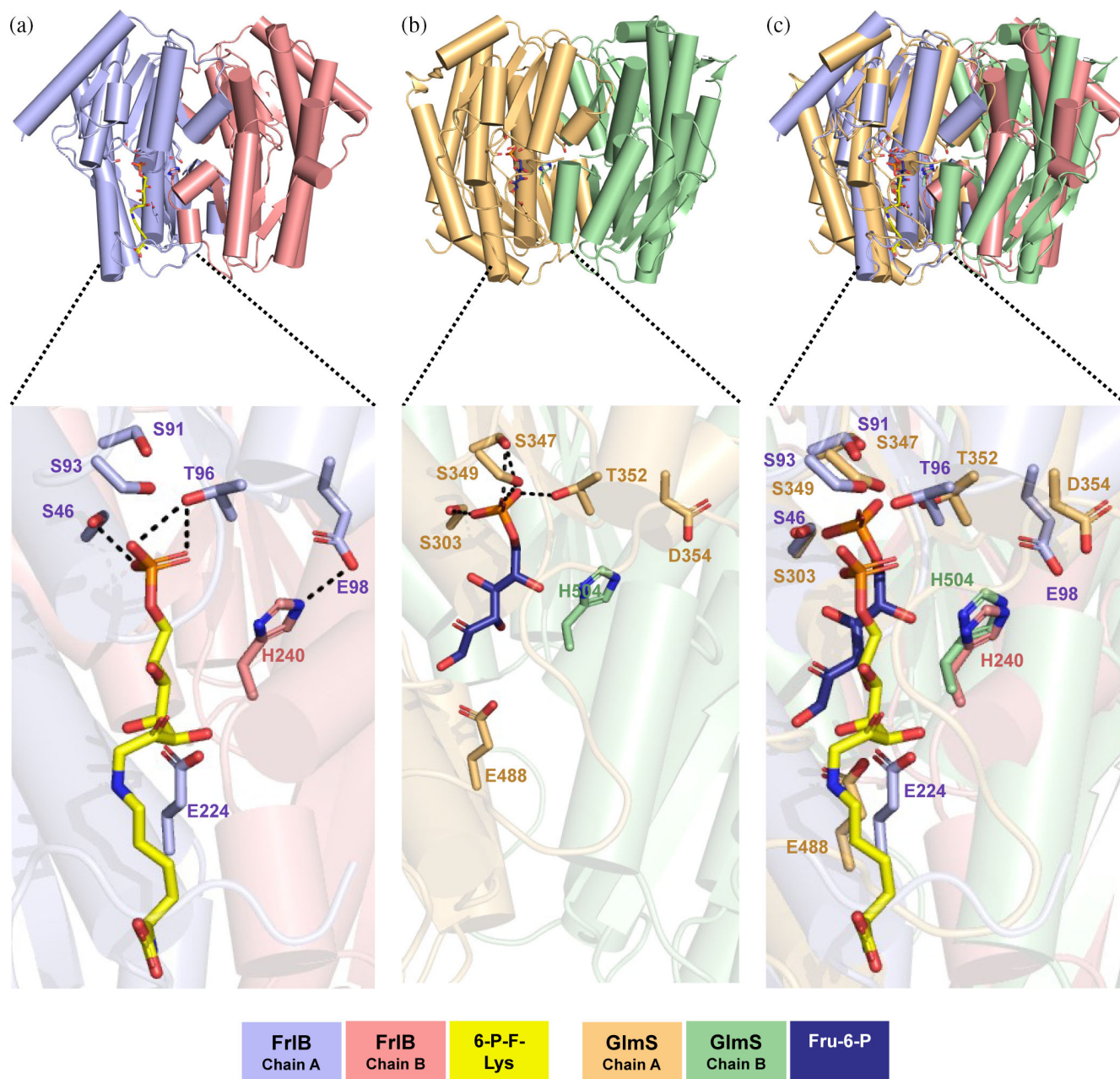
| FrlB Chain A | FrlB Chain B | 6-P-F-Lys | GlmS Chain A | GlmS Chain B | Fru-6-P |

FIGURE 2 Structural similarity between *Salmonella* FrlB and *Escherichia coli* glucosamine-6-phosphate synthase (GlmS). Structure of (a) 6-phosphofructose-lysine (6-P-F-Lys)-docked *Salmonella* FrlB dimer and (b) structure of *E. coli* GlmS bound to Fru-6-P (PDB: 4AMV; Durand et al., 2008) were used to obtain the (c) overlay, which shows the striking similarities between FrlB and GlmS. The bottom insets show magnification of the active sites depicted in (a–c); select conserved residues that interact with the respective substrate are labeled and the putative H-bonds (<3.5 Å) between the phosphate group of the substrate and the amino acid residues are shown in black, dotted lines.

residue that often substitutes for Glu among homologs and offers a good substitute to test the functional significance of the γ-carboxyl group of E224. Using affinity chromatography, we purified all eight FrlB mutants to near homogeneity (Figure S2). We first confirmed the monomeric masses of the wild-type (WT) FrlB and all the mutants using native MS coupled to surface–induced dissociation (SID; Table 2). We then investigated the effect of these mutations on the stability of FrlB. We used

differential scanning fluorimetry (DSF) to determine the thermal denaturation profiles of the FrlB mutant derivatives compared with the WT (Figure S7). The eight mutants can be grouped into four bins: S46A, S91A, S93A, and T96A resemble the T_m of the WT ($T_m = 64°C$); E98A and E224A are slightly less stable than the WT ($T_m = 58°C$); H240A is destabilized ($T_m = 56°C$); and E224Q shows a bimodal behavior with predicted T_m values of 59°C and 74°C. With E224Q, altered polar

TABLE 2 Expected and observed masses of FrlB variants in the absence or presence of substrate.

FrlB sample tested	Monomer (E)		Dimer (E₂)	
	Expected mass (Da)	Observed[a] mass (Da)	Expected mass (Da)	Observed mass (Da)
WT	38,317	38,317[b]	76,634	76,644
WT + S′[c]	38,713	38,711	77,030	77,037
WT + S′₂	—	—	77,426	77,429
WT + P[d]	—	—	76,894	76,910
WT + S′ + P	—	—	77,291	77,302
S46A	38,301	38,301	76,602	76,602
S46A + S′	38,697	38,697	76,998	76,997
S46A + S′₂	—	—	77,394	77,395
S91A	38,301	38,300[b]	76,602	76,603
S91A + S′	38,697	—	76,998	—
S91A + S′₂	—	—	77,394	—
S93A	38,301	38,299	76,602	76,621
S93A + S′	38,697	38,696	76,998	77,010
S93A + S′₂	—	—	77,394	77,400
T96A	38,287	38,286	76,574	76,603
T96A + S′	38,683	38,684	76,970	76,995
T96A + S′₂	—	—	77,366	77,388
E98A	38,259	38,258	76,518	76,548
E98A + S′	38,655	38,659	76,914	76,944
E98A + S′₂	—	—	77,310	77,348
E224A	38,259	38,257	76,518	76,523
E224A + S′	38,655	38,654	76,914	76,915
E224A + S′₂	—	—	77,310	77,314
E224Q	38,316	38,315	76,632	76,632
E224Q + S′	38,712	38,712	77,028	77,033
E224Q + S′₂	—	—	77,424	77,439
H240A	38,251	38,253	76,502	76,525
H240A + S′	38,647	—	76,898	—
H240A + S′₂	—	—	77,294	—

Abbreviations: 6-P-F-Lys, 6-phosphofructose-lysine; Glc-6-P, glucose-6-phosphate; MS, mass spectrometry; WT, wild-type.

[a]These masses were determined using native MS coupled with SID (see Figure S9 for the primary native MS data, Figure S10 for the deconvolved SID spectra, and Figure S11 for the primary SID data).

[b]As additional validation for these monomer masses that were obtained from SID, we also measured the masses of denatured samples of WT and S91A and found that they were in perfect agreement (Figure S13).

[c]S′ represents a 6-P-F-Lys molecule that is bound to two sodium ions and has lost two water molecules (see Figure S12 for supporting evidence).

[d]P refers to Glc-6-P, one of the two products generated by FrlB.

contacts of the Q224 with proximal residues or a decrease in charge repulsion with a proximal E244 residue from the other monomer may have promoted an alternative conformation as evident from its melting profile. In general, two transitions (as with E224Q) with one T_m mirroring that of the native WT fold and another that is higher is indicative of aggregation issues (Gao et al., 2020). While biochemical findings on E224Q must therefore be interpreted with caution, the WT-like behavior and the modest instabilities of the other mutants supported our efforts to forge ahead with activity assays.

To compare the activity of the eight mutants versus the WT FrlB, we used a glucose-6-phosphate dehydrogenase (G6PD)-based coupled assay. We first performed Michaelis–Menten analyses and determined the kinetic parameters of WT FrlB: k_{cat}, 58 ± 2.3 min^{-1} and K_m, 0.6
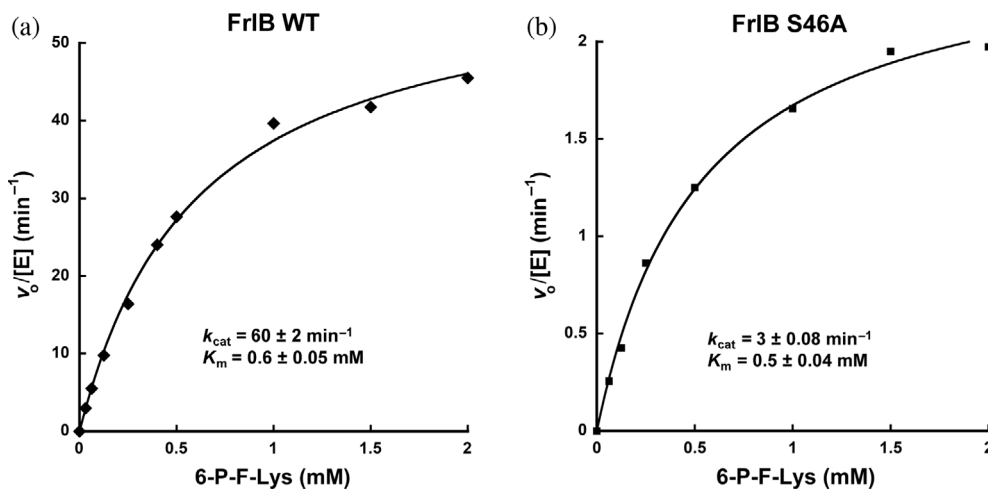
FIGURE 3 Representative Michaelis–Menten analyses for FrlB wild-type (WT) (a) and S46A (b). While the data and fitted k_{cat} and K_m values from only one representative trial for each protein are shown here, two more replicates are included in the Supplementary Material (see Figure S8; text lists mean ± SD from three trials). The errors indicated here for the k_{cat} and K_m values are from the curve-fitting procedure.

± 0.05 mM (mean ± standard deviation calculated from triplicates; Figures 3 and S8); these values are consistent with the data reported for *E. coli* FrlB (Wiame et al., 2002). Surprisingly, besides S46A, none of the FrlB mutants showed any activity even when tested at 30-fold higher concentration than that used in the assay with the WT FrlB (not shown). We were unable to test substrate concentrations >2 mM, as we observed a decrease in WT FrlB activity. With FrlB S46A, we established from our kinetic analyses k_{cat} of 2.3 ± 0.3 min^{-1} and K_m of 0.5 ± 0.04 mM (mean ± standard deviation calculated from triplicates; Figures 3 and S8). Thus, S46 appears to be crucial for positioning the substrate for optimal cleavage, rather than contributing to substrate binding.

2.6 | Mass spectrometric analyses of the FrlB WT and mutants

When any mutant enzyme is inactive, as was the case with seven FrlB mutants, the underlying mutation could have impaired cleavage with or without a substrate-binding defect. Kinetic assays do not distinguish between these two possibilities. Also, methods such as isothermal titration calorimetry (ITC) are not well suited for this purpose if the formation of the ES complex is not accompanied by significant changes in the structure and thermodynamics; for instance, the change in enthalpy may be too small to be measured by ITC. Here, we demonstrate the use of native MS in this regard and showcase its value to determine the ability of FrlB mutants to bind 6-P-F-Lys. Native MS preserves native-like structures of the analytes, retaining noncovalent interactions (Karch et al., 2022; Tamara et al., 2022). These features make native MS suitable for characterizing ES complexes. Moreover, the use of nanoelectrospray ionization in conjunction with SID helps obtain a more accurate monomer mass, yields additional information regarding subunit stoichiometry, and confirms that ES complexes are indeed bona fide by eliminating unproductive ES complexes formed through nonspecific interactions.

The native MS data reveal that WT FrlB binds to 6-P-F-Lys, as evident from the distinct peaks corresponding to E_2S' or $E_2S'_2$ (Table 2, Figures 4a, and S9; corresponding SID data in Figures S10 and S11). We use S' to denote a substrate molecule that is bound to two sodium ions and has lost two water molecules (see Figure S12 for MS data to support this S' assignment). Although we cannot rule out S' as a less active substrate, there are a few reasons why we believe that E_2S' and $E_2S'_2$ are likely surrogates for E_2S and E_2S_2, respectively. First, longer incubations of FrlB with the substrate before native MS-SID dampen the peak intensity of the E_2S' and $E_2S'_2$ complexes (not shown), as would be expected from substrate consumption. Second, the addition of substrate to WT FrlB generates a small amount of E_2P (i.e., FrlB dimer bound to one copy of the Glc-6-P product) and E_2PS' (Figure 4a). Clearly, the FrlB dimer is active before and or during electrospray and productive ES complexes in solution are indeed trapped during the short timeframe of the native MS experiment. Finally, the native MS data obtained with the less active FrlB mutants support the notion E_2S' and $E_2S'_2$ are proxies for E_2S and E_2S_2 (see below).

The S46A mutant, which was the only variant to show catalytic activity at a reduced level (Figure 3), was also capable of binding the substrate, with a distribution of ES' peaks resembling that of the WT (Figure 4b). In fact, we noticed the $E_2S'_2$ peak for S46A to be higher than the E_2 and E_2S' peaks, unlike in the case of WT. This finding suggests that the weaker activity of S46A, compared with WT FrlB, may have lengthened the lifetime of $E_2S'_2$ complexes. The S91A and H240A mutants showed no binding to S', while the remaining five mutants
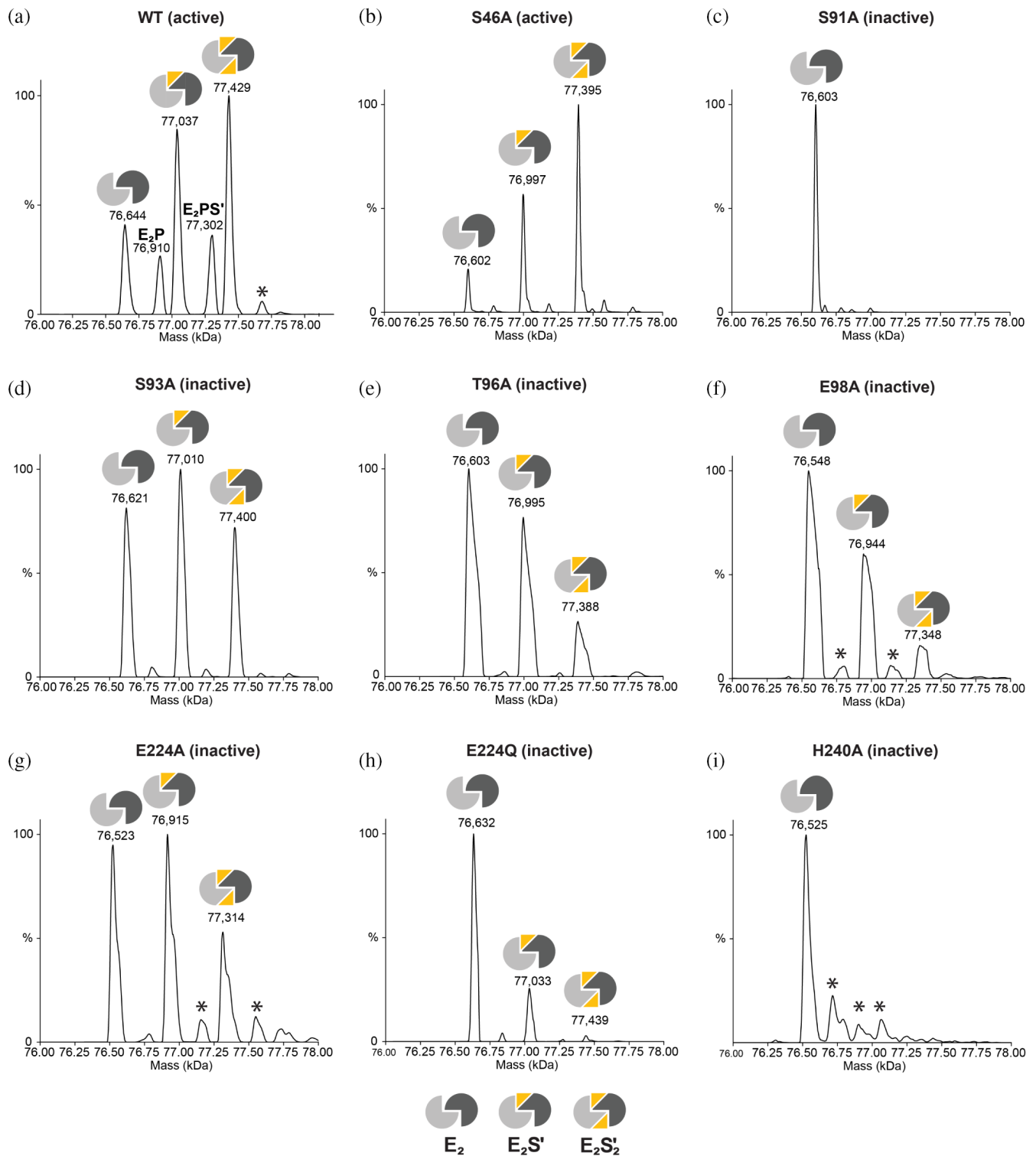
FIGURE 4 Deconvolved native mass spectra for FrlB wild-type (WT) and mutants bound to the substrate, 6-phosphofructose-lysine (6-P-F-Lys; see Figure S9 for the corresponding primary mass spectrometry data). The relevant peaks are annotated using cartoon depictions (E_2, FrlB dimer alone; E_2S' or $E_2S'_2$, FrlB bound to one or two substrate copies, respectively). S' in the figure represents a 6-P-F-Lys molecule that is bound to two sodium ions and has lost two water molecules (see Figure S12 for supporting evidence). Each FrlB mutant derivative is labeled as active or inactive. The spectra for FrlB WT (A) show peaks corresponding to E_2 bound to one copy of the Glc-6-P product (peak labeled as E_2P) and to one copy of the substrate and product (peak labeled as E_2PS'). The scale for the y-axis (relative intensity) is in arbitrary units. Asterisks (*) denote unannotated species.

formed complexes with one or two molecules of S′ (Figure 4c,i). The binding of S′ to E224A (Figure 4g) was expected given that the absence of the general base was predicted to disrupt the cleavage step but not impair substrate binding. However, it was surprising to observe the binding of S′ to S93A with near-WT affinity, because we had hypothesized S93 to be involved in substrate binding (Figure S6). It is possible that S93 assists the binding of the substrate in an optimal orientation, and thus its mutation, while not affecting the binding of the substrate, affects cleavage. The near WT-like binding of S93A (Figure 4d) or the complete absence of binding of S91A (Figure 4c) was unforeseen, considering that they were both predicted to have similar interactions with the phosphate group of the substrate.

The differential behavior between E224A and E224Q with respect to binding to the substrate was intriguing. Our native MS data (Figures 4 and S10) indicate reproducibly stronger binding of S′ to E224A compared with E224Q. One clue as to this unexpected difference emerges from the DSF data, which suggests that E224Q may be structurally altered (Figure S7). We were also surprised by the behavior of E98A and H240A, where we anticipated but did not observe parallels. The FrlB structure revealed a potential electrostatic interaction between H240 in Chain B with E98 in Chain A. We therefore expected that mutating either residue might result in similar destabilization of the dimeric structure. However, the native MS data for H240A revealed the presence of a small monomer population, although this was not the case with E98A (Figure S9I). The basis for this difference as well as their distinctive DSF behavior (Figure S7) may be due to the fact that H240 (unlike E98) is located at the dimeric interface and is involved in inter-subunit interactions.

3 | DISCUSSION

Interactions between enzymes and substrates are expected to alter the conformational equilibrium of both entities during catalysis. To obtain insights into an enzyme's mechanism and associated conformational dynamics, it is typical to investigate a panel of mutants of highly conserved residues and evaluate the functional effects of each mutation. However, when a mutant is less active or inactive compared with the WT, it is often difficult to ascertain if the mutated residue is directly involved in substrate binding or in bond making/breaking. To address this problem with *Salmonella* FrlB, a deglycase involved in F-Lys metabolism, we have taken an integrated structural biology approach. We spotlight below specific insights from our study.

Drawing parallels with other sugar isomerases and FraB (a deglycase), we expect FrlB to operate by coupling an initial isomerization to hydrolysis of a Schiff base (Figure S4). In this mechanism for 6-P-F-Lys deglycation, the protonation of the carbonyl at C2 by a general acid is expected to lower the pKa of one of the C1 hydrogens and thereby permit abstraction of one of the C1 hydrogens by a proximal general base. The resulting enaminol intermediate is converted to a Schiff base, which is then hydrolyzed to Glc-6-P and L-Lys. In the FrlB–6-P-F-Lys docked pose (Figure S6A) that was generated by using the inter-subunit interface as an anchoring constraint, the general base and general acid are E224 of Chain A and H240 of Chain B, respectively. Our activity assays and native MS data obtained with the FrlB E224A mutant, together with previous work on FraB (Sengupta et al., 2019), support the idea that E224 is essential for bond breaking but not substrate binding; in fact, even substitution of an Asp for Glu at the catalytic center (E214D) of FraB resulted in total loss of enzymatic activity, an indication of the exact side-chain carboxyl length necessary for catalysis (Sengupta et al., 2019). FrlB H240A is inactive as was expected based on its postulated role as the general acid but it surprisingly failed to bind the substrate (Figure 4). It is possible that quaternary structure alterations also contribute to this defect, as this was the only mutant that formed a noticeable amount of the monomer (Figure S9I).

While S46, S91, S93, and T96 in FrlB are adjacent to each other and positioned close to the substrate (in the computationally docked pose), mutating these four residues individually resulted in different functional outcomes. Importantly, since the stability of FrlB S46A, S91A, and S93A are nearly the same as WT FrlB (Figure S7), these functional differences are clearly not attributable to gross structural alterations. We analyze below the behavior of these mutants.

FrlB S46A retained its capability to bind to 6-P-F-Lys, as judged by its WT-like K_m (Figure 3) and by native MS (where it was shown to be capable of binding to S′; Figure 4). However, its 25-fold lower k_{cat} suggests that the FrlB conformation associated with substrate binding is different from that used for bond breaking. This contention is supported by two more examples: FrlB S93A and T96A. FrlB S93 and T96 are in the β3–α5 loop that makes contact with 6-P-F-Lys in our docking model (Figure S6). S93A and T96A bound the substrate (Figure 4) but are completely inactive under the conditions that we tested. Because FrlB S46A, S93A, and T96A mutants have E224 and H240 intact, decreased or complete loss of activity could be due to alterations in substrate-binding orientations. Alternatively, if substrate binding is followed by a pre-cleavage conformational

change, the absence of such a trigger may trap the ES complex in an unproductive state. In the case of S91A, we could not detect any substrate binding by native MS. The complete absence of binding with S91A (in contrast to S46A, S93A, and T96A) suggests a hierarchy among various active-site residues all with potential for hydrogen bonding to the hydroxyl, phosphate, and carboxylate moieties in 6-P-F-Lys.

There is a precedent in the F-Lys metabolism context for the total loss of 6-P-F-Lys binding/cleavage by FrlB mutants with single amino acid changes in the substrate-binding site. We present a parallel with the FrlR transcriptional repressor that employs 6-P-F-Lys as the inducer to regulate the F-Lys operon in *E. coli* (Graf von Armansperg et al., 2021). When a luminescence-based reporter assay was used in *E. coli* cells to study the repressor function of WT, S166A, and Y168A FrlR, the five-fold increase in reporter expression observed with the WT was abolished with both mutants. However, no evidence was provided to determine if the S166A and Y168A mutations in the inducer-binding domain of FrlR eliminated binding to 6-P-F-Lys or merely failed to promote a conformational change (postinducer binding) necessary for dissociation of FrlR from the DNA operator.

The native MS data provide convincing evidence for the presence of E_2S' or $E_2S'_2$ in WT FrlB as well the binding-competent FrlB mutant derivatives (Figure 4). However, we do not have information as to whether occupancy of both sites is essential for the deglycase activity of FrlB. To examine if crosstalk between the two catalytic centers in a homodimer is mandatory for function, it will be necessary to examine the activity of heterodimers generated with FrlB mutants in which either the general base or general acid is mutated.

Biological diversity depends on the ability to generate specialist versions of enzymes/proteins that are rooted in an ancestral function. While our findings highlight the common origin of GlmS variants and deglycases, we lack an understanding of the molecular basis for catalytic innovation without a structure of FrlB—6-P-F-Lys. Despite our failure to co-crystallize FrlB and 6-P-F-Lys thus far, we expect improved prospects with FrlB S93A that lacks enzymatic activity but is capable of substrate binding. This optimism is based on the reasoning that if large-scale conformational changes associated with catalysis disrupt the crystal lattice of WT FrlB, a mutant that might not undergo this structural change would yield better crystals of the ES complex.

Overall, the ability to cross-validate our results through multiple approaches has been valuable in understanding the potential roles of active-site residues. The experimental framework used here with FrlB may be useful for future studies involving characterization of enzyme mechanisms.

4 | MATERIALS AND METHODS

4.1 | Overexpression and purification of *Salmonella* FrlB

A codon-optimized gene construct for *Salmonella* FrlB was purchased from GeneUniversal. The FrlB ORF, which was cloned in pET-28b, included an N-terminal His$_6$ affinity tag followed by a tobacco etch virus (TEV) protease-recognition site. This expression plasmid (pET-28b–FrlB) was transformed into *E. coli* BL21(DE3) electrocompetent cells. A single transformant was then inoculated into 2.5 mL of LB media supplemented with 35 μg/mL kanamycin and grown overnight at 37°C in a shaker incubator. The overnight culture was used as a seed culture to inoculate 250 mL of fresh LB medium containing 35 μg/mL kanamycin. The cells were grown at 37°C until the Abs$_{600}$ = 0.6 and then induced for 3 h with 1 mM isopropyl-β-D-thiogalactoside. Post-induction, the cells were harvested by centrifugation and the cell pellets stored at −80°C until further use.

FrlB was purified using immobilized metal affinity chromatography (IMAC). The 250-mL cell pellet from the overexpression was thawed on ice and resuspended in 12.5 mL lysis buffer (97.5% buffer A [50 mM Tris–HCl, pH 7.5, 150 mM NaCl, 1 mM DTT]; 2.5% buffer B [buffer A + 500 mM imidazole]). The lysis buffer was supplemented with a DNase I (40 U, Roche), 10 mM MgCl$_2$, and 1× ProteaseArrest™ protease inhibitor cocktail (G-BioSciences). Following resuspension, the cells were sonicated (50% output power, with 2-s on and 5-s off cycles for a total of 5 min; Ultrasonic Processor, Cole-Parmer) and the resultant crude extract was centrifuged at 24,000 g for 40 min at 4°C. The supernatant was filtered and loaded on to a 1-mL HisTrap column (Cytiva) that had been pre-equilibrated with lysis buffer (albeit lacking DTT).

The HisTrap column was then connected to an ÄKTA FPLC™ Fast Protein Liquid Chromatography (Cytiva) instrument for automated washing and elution. Five milliliter of lysis buffer was used for washing the column, after which a multistep elution gradient was applied using a combination of buffer A and B: 7.5-mL gradient from 50 to 250 mM imidazole, 5-mL gradient from 250 to 500 mM imidazole, and 2.5 mL of 500 mM imidazole. Fractions containing FrlB were identified by SDS-PAGE and Coomassie Blue staining, and those with near-homogenous protein were pooled. This pool was subjected to TEV cleavage (in-house purified His$_6$-TEV: FrlB, 1:20) overnight, while dialyzing at 4°C against 20 mM Tris–HCl (pH 7.5), 150 mM NaCl, and 1 mM DTT.

To remove the His$_6$-tagged TEV protease, uncleaved His$_6$-tagged FrlB, and the cleaved His$_6$ tag, the TEV

protease digestion reaction mixture was bound to Nickel Sepharose High-Performance His$_6$-tagged protein purification resin (GE; binding capacity of 40 mg/mL of resin) which had been pre-washed with double-distilled H_2O and pre-equilibrated with dialysis buffer (lacking DTT). The supernatant was filtered using a 0.22-μm syringe filter and the homogeneity of the final fraction was assessed by SDS-PAGE and Coomassie Blue staining (Figure S2). Corning® Spin-X® UF protein concentrators (5K MWCO) were used to concentrate the proteins when the protein variant was used to set up crystallization trays. A Thermo Scientific NanoDrop-2000 spectrophotometer was used to measure the FrlB concentration ($\varepsilon = 61,100$ M^{-1} cm^{-1}). The purified protein was stored as aliquots at $-80°$C for future use.

4.2 | Crystallization of FrlB

Crystallization trials with 10 mg/mL *Salmonella* FrlB identified several conditions that yielded FrlB crystals, the best of which grew from 0.1 M HEPES (pH 7.5) and 1.0 M ammonium sulfate at 22°C. The hanging drop contained 2 μL of 10 mg/mL FrlB protein mixed with 2 μL of reservoir solution. For data collection, a crystal was transferred to mother liquor supplemented with 30% (vol/vol) glycerol and ammonium sulfate (to ~1.2 M), mounted in a nylon loop, and flash-frozen in liquid nitrogen. X-ray diffraction data were collected using a Rigaku Compact home source equipped with a Copper MicroMax 003f x-ray generator, a PILATUS R200K Hybrid Pixel Array Detector, and an Oxford Cryosystems Cobra cold stream. Diffraction data were integrated and scaled with HKL3000 (Minor et al., 2006). The crystal structure was solved using the molecular replacement method using the MOLREP function in CCP4 (Winn et al., 2011) and PDB: 2A3N as the search model. REFMAC5 (version 5.8.0131) was used for refinement. The atomic model was built using COOT (Emsley et al., 2010) and the structural figures were prepared using PyMOL (The PyMOL Molecular Graphics System, Version 2.4.1. Schrödinger, LLC).

4.3 | MD simulations and docking of 6-P-F-Lys on the structure of FrlB

All docking steps were performed using software available from Schrodinger. The structure of 6-P-F-Lys was built using the 2D sketcher function available in the Maestro GUI (Schrödinger Release 2022–1: Maestro, Schrödinger, LLC). The FrlB model generated from our crystallization studies was used for Receptor Grid Generation 2-based docking. The docking box was designated with a center at the position of the C$_\alpha$ atom of Glu214 in Chain A, with the inner box having dimensions 10 Å × 10 Å × 10 Å and the outer box having dimensions 20 Å × 20 Å × 20 Å. The 6-P-F-Lys substrate was then docked into FrlB along the interface of Glu224 of Chain A and His240 of Chain B using Glide SP (Schrödinger Release 2019-1: Glide, Schrödinger, LLC).

The FrlB dimer without the ligand was used as the starting model for the MD simulations of the free enzyme. After docking 6-P-F-Lys on FrlB, we used this pose as the starting model for MD simulations for the ES model. The 6-P-F-Lys ligand was parameterized for MD using the online server CGenFF (Vanommeslaeghe & MacKerell, 2012), with both starting models subsequently prepared for MD as described in Cool et al. (Cool & Lindert, 2021) Briefly, the systems were solvated using explicit water molecules with NaCl counterions added to neutralize and to establish a salt concentration of 150 mM. The systems were then minimized over two sequential 10,000-step processes, heated up to 310 K over an initial equilibration of 190,000 steps, and then equilibrated during a final 10,000-step process to bring the system into production-run conditions. Fifty-ns MD simulations for both systems were performed using the Owens cluster of the Ohio Supercomputer Center. All preparation steps and MD simulations were conducted using NAMD 2.13 (Phillips et al., 2005) the CHARMM36 force field (Huang & MacKerell, 2013), and a 2-fs timestep. The MD simulations were conducted using an NPT ensemble at 310 K with Langevin temperature and pressure dampening. All bonds with hydrogens were constrained using the ShakeH algorithm which allowed for a 2-fs timestep, with structures being saved every 2 ps.

By analyzing the entire MD simulation trajectory obtained with FrlB alone, we obtained the C$_\alpha$ RMSF of all residues (Figure S6E) as well as the all-atom RMSD of residues in the active site for unliganded and ligand-bound FrlB (Figure S6B,D, respectively). For every frame created during MD simulation of FrlB–6-P-F-Lys, the distance from all atoms in FrlB was determined to each of the atoms in the 6-P-F-Lys substrate. A residue was considered in contact with the ligand if there was a carbon–carbon distance <5.4 Å or any other atom pairings with a distance <4.6 Å (Lindert et al., 2015). The fraction of 25,000 frames with residue-ligand contacts for select residues was then determined (Table S1).

4.4 | Multiple sequence alignments

DeepMSA2 was used to perform the MSAs of *Salmonella* FrlB and *E. coli* GlmS homologs. The primary sequences

were sourced from whole-genome sequence databases (Uniclust30 and UniRef90) and from metagenome databases (Metaclust), BFD, Mgnify, Tara DB, MetaSource DB and IMG/M. A structure model-based MSA ranking pipeline was used as an output choice on the online server. A total of 6,393 FrlB and 13,147 GlmS sequences were used as input for their respective alignments. The sequence logos were generated using WebLogo 3 (Crooks et al., 2004).

4.5 | Construction and purification of FrlB mutant derivatives

The pET-28b–FrlB expression plasmid was used as a template for generating single-site mutants through PCR-based site-directed mutagenesis. For each point mutation, a pair of forward and reverse primers was used to amplify the entire plasmid and introduce the desired mutation (Table S2). The primers were phosphorylated using T4 polynucleotide kinase (New England Biolabs [NEB]) and PCR-based amplifications were performed using PrimeSTAR GXL DNA polymerase (Takara Bio). Following PCR, the template DNA was digested using DpnI and the amplicon was cleaned up using the QIAquick PCR Purification kit (Qiagen). T4 DNA ligase (NEB) was used to circularize the plasmid DNA before electroporation-mediated transformation of *E. coli* DH5α cells. Automated DNA sequencing of mini-prep plasmid DNA was used to confirm the successful construction of the mutant clones.

Each of the eight FrlB mutants was individually transformed into *E. coli* BL21(DE3) cells for overexpression and purification using IMAC (as described above for the WT FrlB). The purity of the eight FrlB mutants was assessed by SDS-PAGE and Coomassie Blue staining (Figure S2).

4.6 | DSF assays

An aliquot of FrlB (WT or mutant) was thawed on ice and a reaction mixture of 28 μL was assembled in a 1.7-mL polypropylene tube with a final concentration of 15 μM protein and 4× SYPRO Orange in DSF buffer (50 mM Tris-Cl [pH 7.5], 150 mM NaCl, 1 mM DTT). The contents were mixed thoroughly through pipetting and 25 μL of the reaction was transferred to a single well in a multi-well plate (Bio-Rad Hard-Shell® 96-Well PCR Plate) and the plate was sealed using a clear microplate seal. The plate was then placed into the PCR machine (CFX96 Touch Real-Time PCR Detection System) and the fluorescence from each well was recorded from 20 to

95°C, with a temperature ramp of 0.5°C per 30 s. To obtain the melting temperature (T_m) for each of the FrlB variants, we plotted the first derivative of the relative fluorescence unit against temperature. For each T_m value that we determined, we calculated the mean and standard deviation from three measurements (Figure S7).

4.7 | Activity assays

The substrate for FrlB, 6-P-F-Lys, was synthesized as previously described (Szkoda et al., 2022). We used a coupled enzyme assay using G6PD (Sigma G6378) to measure FrlB activity. G6PD oxidizes the Glc-6-P generated by FrlB to 6-phosphoglucono-δ-lactone, while simultaneously reducing NAD$^+$ to NADH. The continuous spectrophotometric measurement of NADH produced by G6PD provides a direct readout of the Glc-6-P produced by FrlB. The activity assays with FrlB (WT and mutants) were performed in 25 mM HEPES (pH 7.5), 5 mM MgCl$_2$, 0.1 mM EGTA, and 0.5 mM NAD$^+$. A series of 6-P-F-Lys concentrations were used for the Michaelis–Menten analyses, and the reaction mixtures containing all components (except FrlB) were first incubated at 37°C for 15 min. To this mixture was added FrlB (0.5 μM final concentration) and G6PD (0.075 U/ mL final concentration), each of which had been pre-incubated separately at 37°C for 15 min. From the 30-μL total reaction that was assembled and initiated, 28 μL was immediately transferred to a 384-well microplate and Abs$_{340}$ was monitored continuously using a Biotek Synergy H1 microplate reader (Agilent Technologies). A linear regression analysis of NADH generated as a function of time was used to calculate the initial velocity.

The initial velocity determined at each substrate concentration was subject to the Michaelis–Menten curve-fitting option in Kaleidagraph (Synergy Software) to obtain the respective k_{cat} and K_m values. The curve-fit errors for k_{cat} and K_m did not exceed 4% and 17%, respectively, with R-values >0.99 in all instances. Michaelis–Menten analyses were not performed with the FrlB mutants except S46A because they were inactive even at 15 μM enzyme. Also, we were unable to test substrate concentrations >2 mM, as we observed a decrease in WT FrlB activity.

4.8 | Native MS studies

FrlB samples were buffer exchanged into 200 mM ammonium acetate (Sigma-Aldrich) using a size-exclusion spin column (Micro Bio-Spin 6, BioRad). FrlB concentrations

were determined using Abs_{280} measured with a Nano-drop spectrophotometer (Thermo Scientific). FrlB stocks were then diluted to the desired concentrations (2–4 μM) using 200 mM ammonium acetate. For the characterization of FrlB–6-P-F-Lys complexes, the 6-P-F-Lys stock (in water) was diluted into 200 mM ammonium acetate and then mixed with FrlB immediately before MS measurement (FrlB monomer concentration = 3 μM and 6-P-F-Lys = 150 or 300 μM for the characterization of FrlB–6-P-F-Lys complexes). The sodium that forms S′ appears to be present in the 6-P-F-Lys stock because the native MS of the proteins alone provide more accurate precursor masses of E_2, with E_2 peak shifts to higher m/z occurring upon addition of the 6-P-F-Lys solution.

Native MS experiments were conducted using a Thermo Q Exactive Ultra High Mass Range (UHMR) Orbitrap MS (ThermoFisher Scientific) modified with a 4-cm first-generation SID device (VanAernum et al., 2019). Samples were ionized using a nano-electrospray ionization (nano-ESI) source. Nano-ESI glass capillary tips were pulled in-house using a P-97 micropipette puller (Sutter Instruments). Three to five μL of each sample was loaded into the tips, and the electrospray voltage was set between 0.5 and 0.9 kV. The mass spectrometer was operated under positive mode using the following tunings: capillary temperature: 250°C; detector optimization to low m/z; ion transfer target: high m/z for ES′ complex, low m/z for 6-P-F-Lys; in-source trapping, 30 V; HCD trap gas flow, 5; m/z range, 600–12,000; the resolution was set either 6,250 or 12,500. SID experiments were performed after isolating $E_2S'_2$, with a voltage range from 45 to 65 V, a setting that allowed the dissociation of substrate-bound dimers into monomers with and without 6-P-F-Lys. All the MS runs were performed in duplicate to ensure reproducibility of results. Mass spectra were extracted and examined using Xcalibur 4.1 (Thermo Scientific), and spectral deconvolution was performed using UniDec software (Marty et al., 2015).

ORCID
Steffen Lindert https://orcid.org/0000-0002-3976-3473
Vicki H. Wysocki https://orcid.org/0000-0003-0495-2538
Charles E. Bell https://orcid.org/0000-0001-6486-9408
Venkat Gopalan https://orcid.org/0000-0002-3016-2719

REFERENCES
Bui TP, Ritari J, Boeren S, de Waard P, Plugge CM, de Vos WM. Production of butyrate from lysine and the Amadori product fructoselysine by a human gut commensal. Nat Commun. 2015; 6:10062.

Bui TPN, Troise AD, Nijsse B, Roviello GN, Fogliano V, de Vos WM. *Intestinimonas*-like bacteria are important butyrate producers that utilize Nε-fructosyllysine and lysine in formula-fed infants and adults. J Funct Foods. 2020;70:103974.

Cool AM, Lindert S. Computational methods elucidate consequences of mutations and post-translational modifications on troponin I effective concentration to troponin C. J Phys Chem B. 2021;125:7388–96.

Crooks GE, Hon G, Chandonia JM, Brenner SE. WebLogo: a sequence logo generator. Genome Res. 2004;14:1188–90.

Deppe VM, Bongaerts J, O'Connell T, Maurer KH, Meinhardt F. Enzymatic deglycation of Amadori products in bacteria: mechanisms, occurrence and physiological functions. Appl Microbiol Biotechnol. 2011;90:399–406.

Deppe VM, Klatte S, Bongaerts J, Maurer KH, O'Connell T, Meinhardt F. Genetic control of Amadori product degradation in *Bacillus subtilis* via regulation of *frlBONMD* expression by FrlR. Appl Environ Microbiol. 2011;77:2839–46.

Durand P, Golinelli-Pimpaneau B, Mouilleron S, Badet B, Badet-Denisot MA. Highlights of glucosamine-6P synthase catalysis. Arch Biochem Biophys. 2008;474:302–17.

Emsley P, Lohkamp B, Scott WG, Cowtan K. Features and development of Coot. Acta Crystallogr D Biol Crystallogr. 2010;66: 486–501.

Erbersdobler HF, Faist V. Metabolic transit of Amadori products. Nahrung. 2001;45:177–81.

Erbersdobler HF, Somoza V. Forty years of furosine – forty years of using Maillard reaction products as indicators of the nutritional quality of foods. Mol Nutr Food Res. 2007;51:423–30.

Gao K, Oerlemans R, Groves MR. Theory and applications of differential scanning fluorimetry in early-stage drug discovery. Biophys Rev. 2020;12:85–104.

Graf von Armansperg B, Koller F, Gericke N, Hellwig M, Jagtap PKA, Heermann R, et al. Transcriptional regulation of the N(epsilon)-fructoselysine metabolism in *Escherichia coli* by global and substrate-specific cues. Mol Microbiol. 2021;115: 175–90.

Huang J, MacKerell AD. CHARMM36 all-atom additive protein force field: validation based on comparison to NMR data. J Comput Chem. 2013;34:2135–45.

Karch KR, Snyder DT, Harvey SR, Wysocki VH. Native mass spectrometry: recent progress and remaining challenges. Annu Rev Biophys. 2022;51:157–79.

Lenters-Westra E, Schindhelm RK, Bilo HJ, Slingerland RJ. Haemoglobin A1c: historical overview and current concepts. Diabetes Res Clin Pract. 2013;99:75–84.

Lindert S, Cheng Y, Kekenes-Huskey P, Regnier M, McCammon JA. Effects of HCM cTnI mutation R145G on troponin structure and modulation by PKA phosphorylation elucidated by molecular dynamics simulations. Biophys J. 2015;108:395–407.

Marty MT, Baldwin AJ, Marklund EG, Hochberg GK, Benesch JL, Robinson CV. Bayesian deconvolution of mass and ion mobility spectra: from binary interactions to polydisperse ensembles. Anal Chem. 2015;87:4370–6.

Martysiak-Żurowska D, Stołyhwo A. Content of furosine in infant formulae and follow-on formulae. Pol J Food Nutr Sci. 2007;57:185–90.

McFarland KF, Catalano EW, Day JF, Thorpe SR, Baynes JW. Nonenzymatic glucosylation of serum proteins in diabetes mellitus. Diabetes. 1979;28:1011–4.

Milewski S. Glucosamine-6-phosphate synthase – the multi-facets enzyme. Biochim Biophys Acta. 2002;1597:173–92.

Miller KA, Phillips RS, Kilgore PB, Smith GL, Hoover TR. A mannose family phosphotransferase system permease and associated enzymes are required for utilization of fructoselysine and glucoselysine in Salmonella enterica serovar typhimurium. J Bacteriol. 2015;197:2831–9.

Minor W, Cymborowski M, Otwinowski Z, Chruszcz M. HKL-3000: the integration of data reduction and structure solution – from diffraction images to an initial model in minutes. Acta Crystallogr D Biol Crystallogr. 2006;62:859–66.

Mossine VV, Mawhinney TP. 1-Amino-1-deoxy-D-fructose ("fructosamine") and its derivatives. Adv Carbohydr Chem Biochem. 2010;64:291–402.

Nursten HE. Recent developments in studies of the Maillard reaction. Food Chem. 1981;6:263–77.

Pettersen EF, Goddard TD, Huang CC, Meng EC, Couch GS, Croll TI, et al. UCSF ChimeraX: structure visualization for researchers, educators, and developers. Protein Sci. 2021;30:70–82.

Phillips JC, Braun R, Wang W, Gumbart J, Tajkhorshid E, Villa E, et al. Scalable molecular dynamics with NAMD. J Comput Chem. 2005;26:1781–802.

Sabag-Daigle A, Blunk HM, Sengupta A, Wu J, Bogard AJ, Ali MM, et al. A metabolic intermediate of the fructose-asparagine utilization pathway inhibits growth of a Salmonella fraB mutant. Sci Rep. 2016;6:28117.

Sabag-Daigle A, Boulanger EF, Thirugnanasambantham P, Law JD, Bogard AJ, Behrman EJ, et al. Identification of small-molecule inhibitors of the Salmonella FraB deglycase using a live-cell assay. Microbiol Spectr. 2023;11:e0460622.

Sengupta A, Wu J, Seffernick JT, Sabag-Daigle A, Thomsen N, Chen TH, et al. Integrated use of biochemical, native mass spectrometry, computational, and genome-editing methods to elucidate the mechanism of a Salmonella deglycase. J Mol Biol. 2019;431:4497–513.

Szkoda BE, Di Capua A, Shaffer J, Behrman EJ, Wysocki VH, Gopalan V. Characterization of a Salmonella transcription factor-DNA complex and identification of the inducer by native mass spectrometry. J Mol Biol. 2022;434:167480.

Tamara S, den Boer MA, Heck AJR. High-resolution native mass spectrometry. Chem Rev. 2022;122:7269–326.

Teplyakov A, Obmolova G, Badet B, Badet-Denisot MA. Channeling of ammonia in glucosamine-6-phosphate synthase. J Mol Biol. 2001;313:1093–102.

Teplyakov A, Obmolova G, Badet-Denisot MA, Badet B. The mechanism of sugar phosphate isomerization by glucosamine 6-phosphate synthase. Protein Sci. 1999;8:596–602.

Thirugnanasambantham P, Kovvali S, Cool A, Gao Y, Sabag-Daigle A, Boulanger EF, et al. Serendipitous discovery of a competitive inhibitor of FraB, a Salmonella deglycase and drug target. Pathogens. 2022;11:1102.

Tian W, Chen C, Lei X, Zhao J, Liang J. CASTp 3.0: computed atlas of surface topography of proteins. Nucleic Acids Res. 2018;46:363–7.

van Dongen KCW, Ioannou A, Wesseling S, Beekmann K, Belzer C. Differences in gut microbial fructoselysine degradation activity between breast-fed and formula-fed infants. FEMS Microbiol Ecol. 2022;99:fiac145.

Van Schaftingen E, Collard F, Wiame E, Veiga-da-Cunha M. Enzymatic repair of Amadori products. Amino Acids. 2012;42:1143–50.

VanAernum ZL, Gilbert JD, Belov ME, Makarov AA, Horning SR, Wysocki VH. Surface-induced dissociation of noncovalent protein complexes in an extended mass range orbitrap mass spectrometer. Anal Chem. 2019;91:3611–8.

Vanommeslaeghe K, MacKerell AD. Automation of the CHARMM General Force Field (CGenFF) I: bond perception and atom typing. J Chem Inf Model. 2012;52:3144–54.

Wiame E, Delpierre G, Collard F, Van Schaftingen E. Identification of a pathway for the utilization of the Amadori product fructoselysine in Escherichia coli. J Biol Chem. 2002;277:42523–9.

Wiame E, Duquenne A, Delpierre G, Van Schaftingen E. Identification of enzymes acting on alpha-glycated amino acids in Bacillus subtilis. FEBS Lett. 2004;577:469–72.

Wiame E, Lamosa P, Santos H, Van Schaftingen E. Identification of glucoselysine-6-phosphate deglycase, an enzyme involved in the metabolism of the fructation product glucoselysine. Biochem J. 2005;392:263–9.

Wiame E, Van Schaftingen E. Fructoselysine 3-epimerase, an enzyme involved in the metabolism of the unusual Amadori compound psicoselysine in Escherichia coli. Biochem J. 2004;378:1047–52.

Winn MD, Ballard CC, Cowtan KD, Dodson EJ, Emsley P, Evans PR, et al. Overview of the CCP4 suite and current developments. Acta Crystallogr D Biol Crystallogr. 2011;67:235–42.

Wolf AR, Wesener DA, Cheng J, Houston-Ludlam AN, Beller ZW, Hibberd MC, et al. Bioremediation of a common product of food processing by a human gut bacterium. Cell Host Microbe. 2019;26:463–477.e468.

Wu J, Sabag-Daigle A, Metz TO, et al. Measurement of fructose-asparagine concentrations in human and animal foods. J Agric Food Chem. 2018;66:212–7.

Zhang C, Zheng W, Mortuza SM, Li Y, Zhang Y. DeepMSA: constructing deep multiple sequence alignment to improve contact prediction and fold-recognition for distant-homology proteins. Bioinformatics. 2020;36:2105–12.

SUPPORTING INFORMATION

Additional supporting information can be found online in the Supporting Information section at the end of this article.